Dynamical tipping in a quantum limit cycle

Ya-Xin Xiang,[1] Zhengyang Bai,[1,*] and Yu-Qiang Ma[1,2,†]
[1]*National Laboratory of Solid State Microstructures and School of Physics, Collaborative Innovation Center of Advanced Microstructures, Nanjing University, Nanjing 210093, China*
[2]*Hefei National Laboratory, Hefei 230088, China*

(Received 26 January 2026; accepted 22 June 2026; published 24 July 2026)

Nonequilibrium systems maintain spatiotemporal order through energy dissipation and entropy production. Here, we demonstrate this principle by engineering a quantum limit cycle that emerges from the interplay between a first-order absorbing-state phase transition and feedback mechanism coupling order and control parameters. The quantum limit cycle manifests dynamical correlations driven by multiplicative quantum noise and periodic traverses through tipping points, which act as a robust early-warning signal for state transitions. This periodic crossing results in the enhanced dynamical susceptibility and transient rise of long-range correlations near each tipping event and their subsequent disappearance away from it. These critical transitions are accompanied by a sharp increase in the energy dissipation rate, leading to a stepwise accumulation of dynamical entropy production over time. Our results provide a way for realizing dynamical fluctuations and long-range correlations in strongly interacting driven-dissipative open quantum systems.

DOI: 10.1103/x6rt-7ml3

I. INTRODUCTION

Spontaneous oscillations, known as limit cycles (LCs), are exotic states unique to far-from-equilibrium systems. While extensively studied in classcial system, ranging from chemical and biological models [1–12], they have recently been recognized for their profound resemblance to continuous time crystals in quantum systems [13–27]. In spatially extended systems, the emergence of periodic observables necessitates synchrony among distant constituents, typically achieved through the spontaneous breaking of both spatial and time-translation symmetries [22,28–32]. Although the linear response to fluctuations in LCs has been thoroughly examined [11–13,33–36], a fundamental question persists: Can nonequilibrium fluctuations and dynamical long-range correlations emerge in spatially extended systems in the absence of spatially periodic order?

Here, we demonstrate such a many-body oscillatory state, intrinsically interwoven with long-range correlations, in an open quantum system. Our study is inspired by recent proposals to realize quantum contact processes and absorbing-state phase transitions (APTs) in cold Rydberg gases [37–47]. In this framework, the activation of an emitter is facilitated by its active neighbors [38,43] [see Fig. 1(a)]. Within the quantum regime, the system exhibits bistability, where the order parameter (active population) undergoes a discontinuous jump at the critical threshold of the control parameter (total population). Following the principles of self-organized bistability (SOB) [48,49], we engineer an LC by cycling through the hysteresis loop. This is realized by interfacing the fast transition dynamics with a slow feedback loop on the control parameter [Fig. 1(b)], as detailed in Ref. [50].

The SOB-induced LC is characterized not only by periodic switching between absorbing and active phases but also by oscillatory long-range correlations. Although the LC remains linearly stable, it manifests a transiently diverging dynamical susceptibility. The transition from the absorbing to the active state is marked by a dramatic spike in this susceptibility, where a single activation seed proliferates catastrophically through the system—resembling a wildfire sweeping through a dense forest [see inset, Fig. 1(b)]. This phenomenon is deeply reminiscent of early-warning signals [51–54] observed near tipping points across diverse complex systems, ranging from ecosystems [52,55] and climate dynamics [56] to financial markets [57].

Furthermore, the broken time-translation symmetry is sustained by a continuous exchange of energy with the environment, which offsets the dynamical entropy production [58,59]. Near the tipping point, each transition from the absorbing to the active state is accompanied by a sharp surge in dissipation and a burst of dynamical entropy. In contrast, the entropy production rate vanishes in the frozen absorbing state away from the threshold. Our work thus establishes a fundamental link between driven-dissipative quantum bistability and self-organized spatiotemporal order, highlighting the critical role of tipping points in far-from-equilibrium quantum systems.

II. MODEL

We consider a generic quantum contact model with $|a\rangle$ (active) and $|i\rangle$ (inactive) emitters [38] [see Fig. 1(a)]. The active emitter can spontaneously become inactive (at rate Γ),

*Contact author: zhybai@nju.edu.cn
†Contact author: myqiang@nju.edu.cn

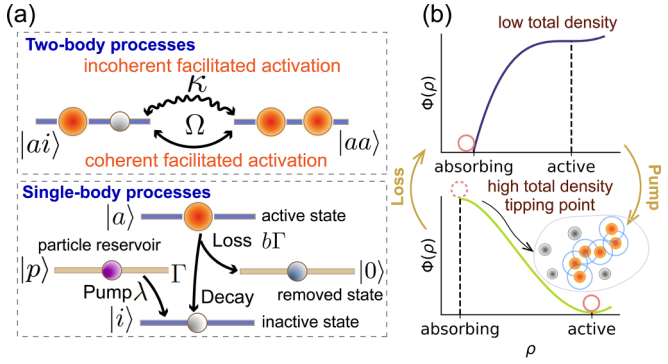

FIG. 1. (a) Effective four-level scheme with timescale separation ($\Gamma, \kappa, \Omega \gg b\Gamma, \lambda$). An inactive quantum emitter (state $|i\rangle$, gray sphere) can be activated via coherent (Ω) and incoherent (κ) facilitated activation by a nearby emitter in the active state $|a\rangle$ (red sphere). Active emitters spontaneously decay either back to $|i\rangle$ or into a removed state $|0\rangle$ (blue sphere), causing emitter loss. Emitters in the pump state $|p\rangle$ (purple sphere) are incoherently transferred to the inactive state to compensate for losses. The system exhibits a first-order APT from a zero-excitation absorbing state to a finite-excitation active state as the total density increases. This is captured by (b) the effective potential $\Phi(\rho)$ for active density ρ at low (top) and high (bottom) total densities. The slow loss and pump processes couple the fast state-switching dynamics to the slow evolution of the total density, generating a limit-cycle state. Within the cycle, a tipping point (dashed red circle) occurs when the absorbing state becomes linearly unstable, allowing a local excitation seed to proliferate throughout the system (inset; facilitation radius marked by a blue circle).

and the inactive one can be activated only in the vicinity of active ones either coherently (at rate Ω) or incoherently (at rate κ).

Under the Markovian noise, the effective dynamics can be described by a Lindblad master equation for the density operator $\hat{\rho}$ ($\hbar = 1$),

$$\partial_t \hat{\rho} = -i[\hat{H}, \hat{\rho}] + \sum_m \mathcal{L}_m \hat{\rho}. \tag{1}$$

The coherent excitation is described by the Hamiltonian

$$\hat{H} = \Omega \sum_l \hat{C}_l \hat{\sigma}_l^x. \tag{2}$$

Here, Ω is the excitation rate, and the local operator $\hat{C}_l = \sum_{k\in\partial l} \hat{\sigma}_k^{aa}$ counts the number of active emitters in the neighborhood of emitter l, where k, l label individual emitters and the summation $\sum_{k\in\partial l}$ runs over the effective nearest neighbors of the lth emitter. The neighborhood is defined by a facilitation shell of radius $R_{\rm fac}$ and thickness $r_{\rm fac}$, such that two emitters are considered neighbors if their separation R lies within the range $[R_{\rm fac} - r_{\rm fac}, R_{\rm fac} + r_{\rm fac}]$ [43].

We define the local transition operators $\hat{\sigma}_l^{\alpha\beta} \equiv |\alpha_l\rangle\langle\beta_l|$ ($\alpha, \beta = a, i, p, 0$) and the Pauli operator $\hat{\sigma}_l^x = \hat{\sigma}_l^- + \hat{\sigma}_l^+$ and $\hat{\sigma}_l^y = i(\hat{\sigma}_l^- - \hat{\sigma}_l^+)$. The latter serves to flip the quantum state via the ladder operators $\hat{\sigma}_l^+ \equiv \hat{\sigma}_l^{ai}$ and $\hat{\sigma}_l^- \equiv \hat{\sigma}_l^{ia}$. The constraint operator $\hat{C}_l$ ensures that spin flips occur only in the presence of a neighboring active emitter, modeling a quantum analog of stochastic branching or coagulation processes [38,50,60].

Local dissipative and incoherent processes are described by Lindblad terms of the form

$$\mathcal{L}_m \hat{\rho} = \sum_l \left[\hat{L}_{m,l} \hat{\rho} \hat{L}_{m,l}^\dagger - \frac{1}{2}\{\hat{L}_{m,l}^\dagger \hat{L}_{m,l}, \hat{\rho}\} \right], \tag{3}$$

where $m \in \{d, p, e, a, b, c, s\}$ labels each distinct process. The spontaneous decay of the active emitters is described by $\hat{L}_{d,l} = \sqrt{\Gamma}\hat{\sigma}_l^-$ with rate Γ, while dephasing of atomic coherences is described by $\hat{L}_{p,l} = \sqrt{\gamma_{\rm de}}\hat{\sigma}_l^{aa}$, with rate $\gamma_{\rm de}$. We further introduce a removed state $|0\rangle$, into which a fraction b of active emitters decay via $\hat{L}_{e,l} = \sqrt{b\Gamma}\hat{\sigma}_l^{0a}$. To compensate for emitter loss, an incoherent pump process $|p\rangle \to |i\rangle$ injects inactive emitters at a constant rate λ, implemented by $\hat{L}_{a,l} = \sqrt{\lambda}\hat{\sigma}_l^{ip}$. This can be realized by laser coupling an auxiliary ground state to the $|p\rangle$ state to achieve population inversion [61,62].

Finally, the incoherent facilitated excitation and decay—corresponding to classical branching and coagulation processes—are incorporated via $\hat{L}_{b,l} = \sqrt{\kappa}\hat{C}_l\hat{\sigma}_l^+$ and $\hat{L}_{c,l} = \sqrt{\kappa}\hat{C}_l\hat{\sigma}_l^-$, respectively, both with rate κ. We also include a weak spontaneous activation at rate $\tau \ll \Gamma$ via $\hat{L}_{s,l} = \sqrt{\tau}\hat{\sigma}_l^+$ (see the Supplemental Material of Ref. [43] for a detailed derivation). This process is only significant near the absorbing state—where the occupation of the active state is exactly zero—and leads to the additional activation term in Eq. (7a).

To characterize the dynamical behavior of the system, we begin with the Heisenberg-Langevin equations of motion for the Pauli and density operators $\hat{\sigma}_l^{x/y/aa}$,

$$\partial_t \hat{\sigma}_l^{aa} = \tau\hat{n}_l - \Gamma\hat{\sigma}_l^{aa} + \Omega\hat{C}_l\hat{\sigma}_l^y + \kappa\hat{C}_l(\hat{n}_l - 2\hat{\sigma}_l^{aa}) + \hat{\xi}_l^{aa}, \tag{4a}$$

$$\partial_t \hat{\sigma}_l^x = -\frac{\kappa\hat{N}_l + \gamma}{2}\hat{\sigma}_l^x - \kappa\hat{C}_l\hat{\sigma}_l^x - \Omega\hat{P}_l\hat{\sigma}_l^y + \hat{\xi}_l^x, \tag{4b}$$

$$\partial_t \hat{\sigma}_l^y = -\frac{\kappa\hat{N}_l + \gamma}{2}\hat{\sigma}_l^y - \kappa\hat{C}_l\hat{\sigma}_l^y + \Omega\hat{P}_l\hat{\sigma}_l^x + 2\Omega\hat{C}_l(\hat{n}_l - 2\hat{\sigma}_l^{aa}) + \hat{\xi}_l^y, \tag{4c}$$

$$\partial_t \hat{n}_l = -b\Gamma\hat{\sigma}_l^{aa} + \lambda\hat{\sigma}_l^{pp} + \hat{\xi}_l^n, \tag{4d}$$

where the local density $\hat{n}_l = \hat{\sigma}_l^{aa} + \hat{\sigma}_l^{ii}$, $\hat{N}_l = \sum_{k\in\partial l}\hat{n}_k$, $\hat{P}_l = \sum_{k\in\partial l}\hat{\sigma}_k^x$, and $\gamma = \Gamma + \gamma_{\rm de}$. The Langevin noise operators $\hat{\xi}_l^{x/y/aa/n}$ are determined by quantum fluctuation-dissipation relations [38,50,63–65].

In the following, we adopt a semiclassical continuum approach, replacing the operator formalism with the respective expectation values. The covariance of the classical Langevin noises derived from the underlying quantum Langevin noise operators is given by $\langle\xi_{l,t}^\nu \xi_{l',t'}^\beta\rangle = \delta(t - t')\delta_{l,l'}\langle\partial_t(\hat{\sigma}_{l,t}^\nu\hat{\sigma}_{l,t}^\beta) - \partial_t(\hat{\sigma}_{l,t}^\nu)\hat{\sigma}_{l,t}^\beta - \hat{\sigma}_{l,t}^\nu\partial_t(\hat{\sigma}_{l,t}^\beta) + \text{H.c.}\rangle$ ($\nu, \beta \in \{x, y, aa\}$), where H.c. stands for the Hermitian conjugate [38,50,63–65]. We focus on the continuum limit, which is justified when the number of atoms within a facilitation sphere is sufficiently large. Under this condition, we define the active and total density fields as $\rho(\boldsymbol{r}, t) \equiv \langle\text{Tr}\{\hat{\sigma}_l^{aa}\hat{\rho}\}\rangle_{\boldsymbol{r}}$ and $n(\boldsymbol{r}, t) \equiv \langle\text{Tr}\{\hat{n}_l\hat{\rho}\}\rangle_{\boldsymbol{r}}$, respectively. Here, $\langle\cdots\rangle_{\boldsymbol{r}}$ designates a spatial

average over a facilitation sphere centered at position $\boldsymbol{r}$ [50]. The coherence fields, $\sigma^{x/y}$, are defined similarly.

Based on the resultant Langevin equations for these classical fields, we further perturbatively eliminate the fast coherence fields $\sigma^{x/y}$ via the Janssen-De Dominicis-Martin-Siggia-Rose procedure [66–69]. This procedure, valid under quantum dephasing and weak driving, yields a path integral for the active density field [50],

$$\mathcal{Z} = \int \mathcal{D}[\rho, \tilde{\rho}] e^{-\mathcal{S}[\rho,\tilde{\rho}]}, \tag{5}$$

with the action

$$\mathcal{S}[\rho, \tilde{\rho}] = \int \tilde{\rho}[(\partial_t - D_\rho \nabla^2 + u_2)\rho + u_3\rho^2 + u_4\rho^3 - \mu\tilde{\rho}] \tag{6}$$

and the coupled Langevin equations for active and total densities [50],

$$\partial_t \rho = D_\rho \nabla^2 \rho - u_2\rho - u_3\rho^2 - u_4\rho^3 + \tau n + \xi_\rho, \tag{7a}$$

$$\partial_t n = D_{\mathrm{T}} \nabla^2 n - b\rho + \lambda + \xi_n. \tag{7b}$$

Here, the coefficients are given by $u_2 = 1 - n\kappa - 256n^2\Omega^4/(n\kappa + \gamma)^7$, $u_3 = 2[\kappa - 2n\Omega^2/(n\kappa + \gamma)]$, and $u_4 = 8\Omega^2/(n\kappa + \gamma)$. The terms ξ_ρ and ξ_n represent Gaussian white noises with zero mean, characterized by the variance-covariance matrix elements $M_{\rho\rho} = (1 + n\kappa)\rho + 4n\Omega^2\rho^2/(n\kappa + \gamma)^2 = 2\mu$ and $M_{nn} = b\rho$. Furthermore, the effective diffusion constant is defined as $D_\rho = D_{\mathrm{T}} + n\kappa R_{\mathrm{fac}}^2/2$, where D_{T} accounts for the thermal diffusivity.

III. RESULTS

A. Effective local potential for active density

With the total density n held fixed, the active-density equation (7a) defines an effective local potential $\Phi(\rho)$ conditioned on n. Omitting spatial fluctuations, variation with respect to ρ and $\tilde{\rho}$ yields the Hamilton-Jacobi equations [70]

$$\partial_t \tilde{\rho} = -\partial_\rho H_{\mathrm{cl}} = \tilde{\rho}(u_2 + 2u_3\rho + 3u_4\rho^2) - \tilde{\rho}^2(\mu_1 + 2\mu_2\rho), \tag{8a}$$

$$\partial_t \rho = \partial_{\tilde{\rho}} H_{\mathrm{cl}} = -(u_2\rho + u_3\rho^2 + u_4\rho^4) + 2\mu\tilde{\rho}. \tag{8b}$$

Here, the density-dependent coefficient is given by $\mu = \mu_1\rho + \mu_2\rho^2$, with $\mu_1 = (1 + n\kappa)/2$ and $\mu_2 = 2n\Omega^2/(n\kappa + \gamma)^2$. The corresponding classical Hamiltonian, H_{cl}, is expressed as

$$H_{\mathrm{cl}} = -\tilde{\rho}(u_2\rho + u_3\rho^2 + u_4\rho^3) + \mu\tilde{\rho}^2. \tag{9}$$

The increment of the action along the optimal path (with $H_{\mathrm{cl}} = 0$) described in Eq. (8) connecting a pair of noiseless ($\tilde{\rho} = 0$) states is defined as the difference in the effective local potential between them [71].

By defining the absorbing state (with $\rho = 0$) as the reference point where the potential vanishes [$\Phi(\rho = 0) = 0$], the effective local potential for an arbitrary state is given by

$$\begin{aligned}\Phi(\rho) &= \int_0^\rho dx \left\{ \frac{u_2 x + u_3 x^2 + u_4 x^3}{\mu_1 x + \mu_2 x^2} \right\} \\ &= \frac{u_4}{\mu_2}\left[\frac{\rho^2}{2} + \left(\frac{u_3}{u_4} - \frac{\mu_1}{\mu_2}\right)\rho\right] \\ &\quad + \frac{u_4}{\mu_2}\left[\frac{u_2}{u_4} + \frac{\mu_1}{\mu_2}\left(\frac{\mu_1}{\mu_2} - \frac{u_3}{u_4}\right)\right] \ln(\mu_2\rho + \mu_1).\end{aligned} \tag{10}$$

Typical effective local potential curves for low and high total densities are shown in Fig. 1(b). At low total density n, the system favors the absorbing state, whereas high n shifts the equilibrium toward the active state. The interplay between slow loss (at rate $b\Gamma$) and pumping (at rate λ) couples the fast transition dynamics to the slow evolution of the total density, triggering an LC phase along the hysteresis loop of a first-order APT, as described in detail below.

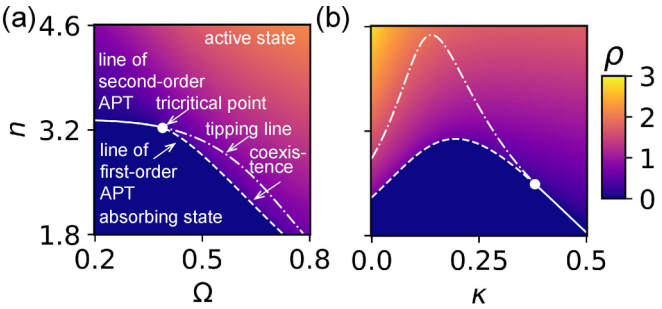

FIG. 2. Mean-field (MF) phase diagrams for (a) $\kappa = 0.3$ and (b) $\Omega = 0.5$ at fixed total density n. Color indicates the active density ρ. In the classical (quantum) regime, the system exhibits a second-order (first-order) APT from the absorbing with $\rho = 0$ to an active state with finite ρ, marked by solid (dashed) lines. The two transitions meet at a tricritical point (dot). Within the first-order APT regime, the tipping point (dash-dotted lines) marks where the absorbing state becomes linearly unstable ($u_2 = 0$). The region between the tipping line and the first-order APT line is a coexistence regime where the absorbing and active states are both stable.

B. First-order absorbing-state phase transition and tipping point

Based on the effective action (6) for the active density, we obtain the MF phases by identifying the noiseless saddle-point solutions at a fixed total density n. The corresponding phase boundaries are illustrated in Fig. 2. In the quantum regime ($\Omega > \kappa$), the excitation density changes discontinuously from zero to a finite value as the total density n crosses a critical threshold (dash-dotted line), marking a first-order APT. This discontinuous jump forms a key ingredient of the SOB-induced LCs discussed later. As the classical activation rate κ increases, the system enters a classical regime characterized by a second-order transition (solid line), consistent with self-organized criticality in driven-dissipative Rydberg gases [42,43,72].

In the coexistence regime, further increase of the total density destabilizes the absorbing state. This behavior is captured by the linear coefficient u_2, which characterizes the inverse recovery rate of a homogeneous system near the absorbing

state. When $u_2 > 0$, the absorbing state is linearly stable and fluctuations in the active-density fields dampen over time. In contrast, $u_2 < 0$ indicates linear instability, where even an infinitesimal perturbation can trigger an abrupt surge in the active density. The susceptibility of the system is also manifested in the spatial propagation of an active seed. To quantify this, we analyze the spatiotemporal fluctuations of the active-density field at a fixed total density n. Linearizing Eq. (7a) near the absorbing state $\rho_{0,t} = 0$ and performing a Fourier transform yields the following evolution equation:

$$\partial_t \delta\rho_{\boldsymbol{k},t} = -(k^2 + u_2)\delta\rho_{\boldsymbol{k},t} + \xi_\rho. \tag{11}$$

Consider an initial configuration where all sites are absorbing except for a single seed localized at $\boldsymbol{r}_0$, expressed as $\rho_{\boldsymbol{r},t=0} = a_0\delta(\boldsymbol{r} - \boldsymbol{r}_0)$, with $0 < a_0 \ll 1$. Applying a Laplace transform leads to

$$(k^2 + u_2 + i\omega)\delta\rho_{\bar{\omega}} = \xi_\rho + a_0 e^{-i\boldsymbol{k}\cdot\boldsymbol{r}_0}, \tag{12}$$

where the shorthand notation $\bar{\omega} = (\omega, \boldsymbol{k})$. After averaging over the noise and performing the inverse Fourier transform, the real-space dynamics are given by

$$\frac{\langle\delta\rho_{\boldsymbol{r},t}\rangle}{a_0} = \int d\bar{\omega}\frac{e^{i[\omega t + \boldsymbol{k}\cdot(\boldsymbol{r}-\boldsymbol{r}_0)]}}{k^2 + u_2 + i\omega} \propto \frac{e^{-\frac{|r-r_0|^2}{4t} - u_2 t}}{t^{d/2}}, \tag{13}$$

where d denotes the spatial dimension. Consequently, for $u_2 > 0$, the activation remains exponentially localized within a characteristic length scale of $\xi \sim u_2^{-1/2}$. In contrast, for $u_2 < 0$, the initial seed proliferates, leading to a spreading activation front across the entire system.

Consequently, within the first-order APT regime, any parameter $x \in \{n, \Omega, \kappa\}$ satisfying $u_2 = 0$ identifies a tipping point [52,53,56,73], marking the onset of propagating activation seeds (represented by dash-dotted lines in Fig. 2). Our analysis focuses on this threshold while disregarding the secondary transition from the active to the absorbing state (the dashed lines in Fig. 2). Unlike the correlated collective activation that drives the tipping point, the latter is governed merely by stochastic, local, and uncorrelated inactivation events.

C. The realization of limit-cycle state

In the regime of first-order APTs, introducing loading and loss processes couples the dynamics of the active density to its control parameter, the total density. Within the coexistence regime, as illustrated in Fig. 3(a), the fixed point of the equation for total density (7b) can be either stable or unstable fixed point of the equation for active density (7a), depending on the loading rate λ. A critical loading rate, λ_c, is defined as the condition where the steady-state active density that nullifies Eq. (7b) coincides with the active density at the critical total density of the first-order phase transition (represented by the black dashed line). This critical loading rate demarcates two distinct regimes: a stationary state for $\lambda > \lambda_c$ [Fig. 3(b)] and an LC regime for $\lambda < \lambda_c$ [Fig. 3(c)].

In Eq. (7a), a weak, rare spontaneous activation process at a rate $\tau \ll \kappa, \Omega$ prevents the system from being permanently trapped in the absorbing state. Without this term, the activation dynamics would cease, resulting in overloading. Once the absorbing state is reached, this rare process restores the

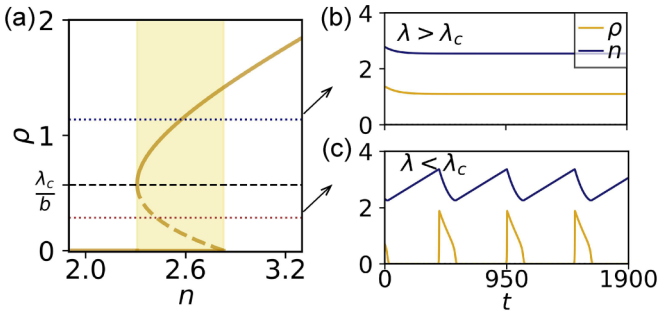

FIG. 3. MF picture of limit cycle state induced by self-organized bistability. (a) For a given loading rate λ, the stationary solution to the coupled equations (7a) and (7b) corresponds to the intersection between the yellow curve [fixed points of the active-density equation (7b) at fixed total density; solid/dashed segments indicate stable/unstable branches] and the horizontal dashed line [fixed point of total-density equation (7b)]. The coexistence regime is shaded yellow. A critical loading rate λ_c separate two regimes: (b) limit-cycle state for $\lambda < \lambda_c$ and (c) stationary state for $\lambda > \lambda_c$.

dynamics over a characteristic timescale of $(\tau N)^{-1}$, where N is the total number of emitters. This mechanism counteracts potential overloading and is essential for sustaining long-term phase coherence in finite-sized systems [50].

Furthermore, in finite dimensions, the robustness of these LCs is intimately linked to the underlying first-order transition; consequently, they are expected to persist for $d \geqslant 2$ [50]. For simplicity, the following analysis focuses on the three-dimensional case where stable LCs have been established, using the parameter set D_T, $D_\rho = 1$, $\kappa = 0$, $\Omega = 0.5$, $\gamma = 2$, $\tau = 10^{-7}$, and $b = 10^{-2}$.

D. Linear stability of limit-cycle state

We now demonstrate that the tipping point triggers instantaneous long-range correlations without compromising the stability of the LC. To investigate this, we consider the fluctuations $\delta\rho_{\boldsymbol{r},t}$ and $\delta n_{\boldsymbol{r},t}$ around the MF trajectory $(\rho_{0,t}, n_{0,t})$ within a Gaussian approximation. By expanding Eqs. (7a) and (7b) and performing a Fourier transform, we define the fluctuation fields as $\delta\rho_{\boldsymbol{k},t} = \rho_{\boldsymbol{k},t} - \rho_{0,t}$ and $\delta n_{\boldsymbol{k},t} = n_{\boldsymbol{k},t} - n_{0,t}$. The linearized equations of motion for the correlation functions, written in the vector form $\boldsymbol{C}_{k,t} = (\langle\delta\rho_{\boldsymbol{k},t}\delta\rho_{-\boldsymbol{k},t}\rangle, \quad \langle\delta\rho_{\boldsymbol{k},t}\delta n_{-\boldsymbol{k},t}\rangle, \quad \langle\delta n_{\boldsymbol{k},t}\delta n_{-\boldsymbol{k},t}\rangle)^T$, are governed by

$$\partial_t \boldsymbol{C}_{k,t} = \boldsymbol{L}_{k,t}\boldsymbol{C}_{k,t} + 2\boldsymbol{M}_{k,t}, \tag{14}$$

where the superscript "T" denotes the transpose, and the noise covariance vector is $\boldsymbol{M} = (M_{\rho\rho}, \quad 0, \quad M_{nn})^T$. The linear response matrix $\boldsymbol{L}(k,t)$ is derived from the Jacobian matrix $J_{\alpha\beta} = (\partial_\beta F_\alpha)_0 - \delta_{\alpha,\beta}k^2$ (with $\alpha, \beta \in \{\rho, n\}$), where F_ρ and F_n represent the deterministic components of Eqs. (7a) and (7b), respectively. The subscript "0" indicates evaluation along the MF values $\rho = \rho_{0,t}$ and $n = n_{0,t}$. The matrix $\boldsymbol{L}$ is then explicitly given by

$$\boldsymbol{L} = \begin{pmatrix} 2J_{\rho\rho} & 2J_{\rho n} & 0 \\ J_{n\rho} & J_{\rho\rho} + J_{nn} & J_{\rho n} \\ 0 & 2J_{n\rho} & 2J_{nn} \end{pmatrix}. \tag{15}$$

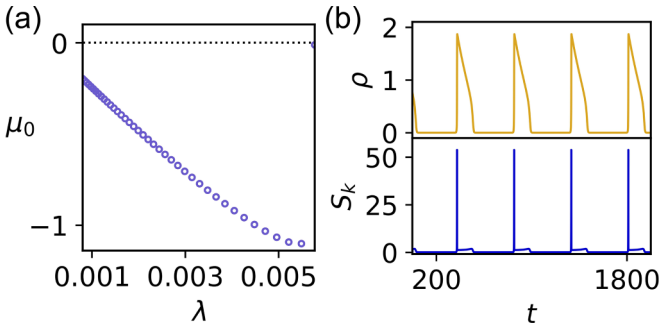

FIG. 4. (a) Floquet multiplier that corresponds to fluctuations of active-density fields with respect to MF trajectory as a function of λ for $k = 0$. (b) The dynamical behavior of the active density (upper) and correlation function (lower) $S_k = \langle \delta\rho_{\boldsymbol{k},t}\delta\rho_{-\boldsymbol{k},t}\rangle$ within Gaussian approximation for $k = 0.1\pi$. In line with a negative Floquet multiplier in panel (a), the correlation function S_k is periodic and finite with peaks corresponding to the tipping point, where the system is about to jump from the absorbing state toward the absorbing state and is therefore susceptible to fluctuations.

Due to the time periodicity of $\rho_{0,t}$ and $n_{0,t}$, the drift matrix $\boldsymbol{L}$ and the diffusion vector $\boldsymbol{M}$ are inherently time dependent. Consequently, the correlation functions $\boldsymbol{C}_{k,t}$ also exhibit corresponding temporal oscillations. Given that the dynamics of the active and total density fields occur on widely separated timescales, we can employ a separation of variables approach. By neglecting all correlation components in Eq. (14) except for the active-density autocorrelation $S_{k,t} = \langle \delta\rho_{\boldsymbol{k},t}\delta\rho_{-\boldsymbol{k},t}\rangle$, the evolution simplifies to

$$\partial_t S_{k,t} = 2J_{\rho\rho}S_{k,t} + 2M_{\rho\rho}. \tag{16}$$

For the mth period, defined as $t \in ((m-1)T, mT]$, with T being the limit cycle period, the formal solution under the initial condition $S_{k,0} = 0$ is given by

$$\begin{aligned} S_{k,t} &= 2\int_0^t dx M_{\rho\rho}(x) e^{2\int_x^t dy J_{\rho\rho}(y)} \\ &= 2\left(\sum_{l=0}^{l=m-1}\int_{lT}^{(l+1)T} + \int_{mT}^{t}\right) dx \left\{ M_{\rho\rho} e^{2\int_x^t dy J_{\rho\rho}} \right\} \\ &= S_{k,t-mT} + 2e^{\int_0^{t-mT} dx J_{\rho\rho}(x)} S_{k,T} \frac{1-e^{mT\mu_k}}{1-e^{T\mu_k}}, \end{aligned} \tag{17}$$

where the Floquet multiplier [11–13,33,74] is given by

$$\mu_k = \frac{2}{T}\int_0^T dx J_{\rho\rho}(x) = \mu_0 - 2k^2. \tag{18}$$

It follows from Eq. (17) that the LC becomes unstable if $\mu_k \geqslant 0$ for any k.

The zero-mode Floquet multiplier μ_0 (at $k = 0$), obtained via numerical integration of Eq. (18), is presented in Fig. 4(a). Notably, μ_0 remains negative throughout the parameter regime where the LC exists. Since $\mu_k < \mu_0$ for all $k > 0$, all finite-k modes are likewise stable. Consequently, the correlation function $S_{k,t}$ remains bounded, consistent with the results from the direct numerical integration of Eq. (16) [see Fig. 4(b)].

As illustrated in Fig. 4(b), S_k manifests a sharp peak within each period, signaling a transient but pronounced enhancement in the system's response to perturbations (lower panel) immediately prior to the transition from the absorbing to the active state (upper panel). As discussed in the previous section, this enhanced sensitivity to fluctuations coincides with the linear instability of the absorbing phase, which occurs when the total density n satisfies $J_{\rho\rho}|_{\rho=0} = u_2(n) = 0$. This condition corresponds precisely to the tipping point indicated by the dash-dotted lines in Fig. 2. At this point, the system reacts strongly to fluctuations in the active field, triggering an abrupt surge in the active density. Importantly, this phenomenon does not signify an instability of the LC itself; rather, it reflects a dramatic spike in dynamical susceptibility during the switching from the absorbing to the active state.

In the following, we present the results obtained from numerical simulations of Eqs. (7a) and (7b). These simulations employ an operator-splitting scheme [50,75,76] to ensure numerical stability and accuracy.

E. State-dependent entropy production rate

LCs are nonequilibrium species that break time-translation invariance. To sustain such dynamical asymmetry, these systems require a continuous influx of energy and a persistent rate of entropy production [58,77]. In this context, entropy associated with the breaking of time-reversal symmetry is defined as dynamical entropy, distinguishing it from the static entropy related to spatial symmetries. This dynamical entropy provides a rigorous measure of path irreversibility, typically expressed as the log ratio between the probabilities of forward and time-reversed trajectories [78]. Correspondingly, the steady-state entropy production rate per unit volume, arising from the dynamics of the active-density field, is defined as

$$\partial_t S(t) = \frac{1}{L^d}\sum_l \int \frac{d\rho d\rho'}{dt} p_{l,t}(\rho,\rho') \ln\left[\frac{p_{l,t}(\rho,\rho')}{p^{\mathrm{R}}_{l,t}(\rho',\rho)}\right]. \tag{19}$$

In this expression, $p_{l,t}(\rho,\rho')$ represents the probability for a local trajectory at site l to evolve from ρ to ρ' over a short interval dt. The superscript "R" specifies the time-reversed trajectory.

In the steady state, spatial translation invariance allows the marginal probability to be expressed as $p_{l,t}(\rho,\rho') = \int dn P^{\mathrm{SS}}_t(n,\rho) P(\rho \to \rho')$, where $P^{\mathrm{SS}}_t(n,\rho)$ is the steady-state probability density of average total and active densities at time t, and $P(\rho \to \rho')$ is the short-time propagator associated with the Langevin equation (7a). Within the Onsager-Machlup framework [66–69], this transition probability takes a Gaussian form:

$$P(\rho \to \rho') = \frac{1}{\sqrt{2\pi M_{\rho\rho}dt}} \exp\left[-\frac{(\rho'-\rho-F_\rho dt)^2}{2M_{\rho\rho}dt}\right], \tag{20}$$

where the deterministic drift F_ρ is evaluated at the initial state ρ. Its time-reversed counterpart $P^{\mathrm{R}}(\rho' \to \rho)$ is obtained by exchanging the initial and final states while maintaining the functional form of the drift. The backward path probability is thus $p^{\mathrm{R}}_{l,t}(\rho',\rho) = \int dn P^{\mathrm{SS}}_t(n,\rho) P^{\mathrm{R}}(\rho' \to \rho)$ [78]. By substituting the stochastic evolution $\rho' = \rho + (F_\rho + \xi_\rho)dt$ into the definition of the entropy production rate (19), we arrive at the

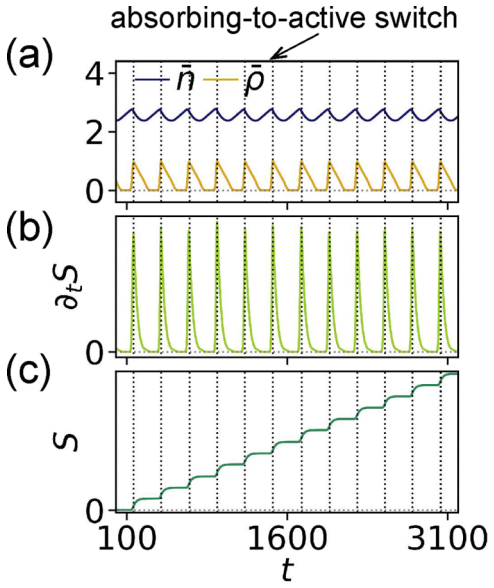

FIG. 5. Time series of (a) the spatially averaged total $\bar{n}$ and active $\bar{\rho}$ densities, (b) instantaneous entropy production rate $\partial_t S$, and (c) total entropy production S. Gray dashed lines mark transitions from the absorbing to the active state. The instantaneous entropy production rate peaks at the tipping point where the system switches from the absorbing to active states. Parameters for panels (a)–(c) are $L = 64$ and $\lambda = 3.2 \times 10^{-3}$.

following integral expression:

$$\partial_t S(t) = \int d\rho dn d\xi_\rho \frac{e^{-\frac{\xi_\rho^2}{2M_{\rho\rho}}}}{\sqrt{2\pi M_{\rho\rho}}} P_t^{\mathrm{SS}}(n,\rho) \frac{2F_\rho(F_\rho + \xi_\rho)}{M_{\rho\rho}}. \tag{21}$$

After integrating over the noise ξ_ρ, the entropy production rate simplifies to the following form:

$$\partial_t S(t) = 2\left\langle \frac{F_\rho^2}{M_{\rho\rho}} \right\rangle_l, \tag{22}$$

where $\langle \cdots \rangle_l$ denotes the spatial average over all sites. This expression corresponds to the generalized energy dissipation rate for the overdamped Langevin dynamics in Eq. (7a). Specifically, it represents the ratio of the squared generalized force to its associated diffusion coefficient [68,79,80]. Consequently, this result highlights the fundamental balance between entropy production and energy dissipation within the system's nonequilibrium steady state.

Temporal integration of the entropy production rate, $\partial_t S$, yields the total accumulated entropy, S. As illustrated in Fig. 5(b), the entropy production rate exhibits a sharp peak during the transition from the absorbing to the active state, which manifests as a characteristic steplike rise in the accumulated entropy S [Fig. 5(c)]. In regions away from this transition, the entropy production increases only marginally and remains nearly stationary within the absorbing state. This intermittent burst of entropy production serves as a thermodynamic signature of the discontinuous switching process, reflecting the dissipative cost required to cross the tipping point manifold.

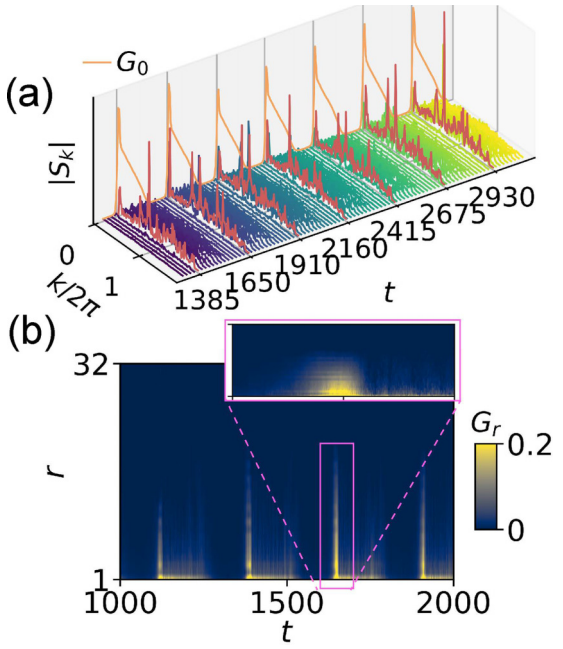

FIG. 6. Dynamical spatial correlations of limit-cycle state. (a) Amplitude of the pairwise correlation functions of the active-density field in Fourier space, $|S_k|$, colored by time. The curve is highlighted in red when the absorbing-to-active transition occurs (also marked by gray lines therein). The autocorrelations G_0 are colored in orange. (b) Temporal behavior of real-space correlation functions G_r (color coded) where the insert provides an enlarged view of how long-range correlations emerge and disappear as the system crosses the tipping point enclosed by the magenta frame. Parameters for panels (a) and (b) are $L = 64$ and $\lambda = 3.2 \times 10^{-3}$.

F. Dynamical spatial correlations

Building upon the analysis of global correlations and entropy production, we now examine the spatial organization of the system. This is quantitatively assessed through two-point spatial correlation functions, which reveal the underlying structural order and collective behavior. Due to the system's invariance under rotation and displacement, the real-space correlation function $G_{r,t}$ depends solely on the relative distance r,

$$G_{r,t} = \langle \delta\rho_{l,t}\delta\rho_{k,t}\delta(r - |\boldsymbol{r}_l - \boldsymbol{r}_k|)\rangle_{l,k}, \tag{23}$$

whose Fourier transform yields the static structure factor $S_{k,t}$ [79]. Under the assumption that nonlocal correlations are subordinate to those induced by quantum noise, the steady-state autocorrelation can be estimated as $G_0 \approx \bar{\rho}/2d$.

Transitions from the absorbing to the active state are accompanied by sharply enhanced spatial correlations, as illustrated in Figs. 6(a) and 6(b). These results align with our Gaussian analysis, where the dynamical instability near the tipping point—manifesting as a sudden surge in active density—triggers a transiently heightened susceptibility to perturbations [Fig. 4(b)]. As the system approaches and then passes the tipping point, the rapid proliferation of active emitters and the concomitant emergence of long-range correlations resemble a wildfirelike spread through a dense emitter network. This burst of collective activation is subsequently

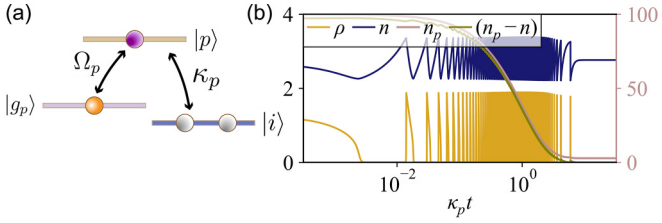

FIG. 7. (a) Level scheme for pump process. Emitters are optically driven from the auxiliary ground state $|g_p\rangle$ to the pump state $|p\rangle$, which then transfers population to the inactive state $|i\rangle$ via an incoherent coupling with strength κ_p. (b) MF time series of active (ρ), total (n), and pump (n_p) particle densities for the quantum limit cycle. The left axis shows ρ and n; the right axis shows n_p and its difference from total density $(n_p - n)$. Time is rescaled by the pumping rate (incoherence coupling rate) $\kappa_p = \lambda/n_p(t = 0)$, with initial reservoir density $n_p(0) = 100$ and injection parameter $\lambda = 3.2 \times 10^{-3}$.

quenched by the depletion of the emitter population, leading to the eventual disappearance of long-range order.

G. Experimental implementation

Finally, we discuss potential experimental implementations. The proposed model can be realized using coherent laser-driven Rydberg atoms in the facilitation (antiblockade) regime. In this setup, the electronic ground and Rydberg states are mapped to the inactive and active states, respectively, while additional auxiliary levels can represent the removed state [38,42,43,47]. The facilitation radius in our model corresponds to the Rydberg blockade radius. Since our framework focuses on two-body contact processes, its validity holds for densities where at least two Rydberg atoms reside within a single facilitation sphere. Furthermore, the relative weight between coherent and incoherent activation can be tuned via the driving lasers.

Meanwhile, the injection of inactive emitters can be implemented via atomic pumping using Raman processes [61,62]. The pump state $|p\rangle$ is initially prepared by laser coupling an auxiliary ground state $|g_p\rangle$ to $|p\rangle$ to achieve a population inversion, thereby establishing the initial population $n_p(t = 0)$, and pump process is then realized through an incoherent coupling between $|p\rangle$ and $|i\rangle$ [see Fig. 7(a)]. In a real experimental setup, however, the population in the pump state will eventually deplete over time. If the system is initialized with a high population in the pump state and a low pumping rate κ_p, the limit cycle can last for many cycles. This is demonstrated in Fig. 7(b), where we initialize the system with a high pump-state density $n_p(0) = 100$ (corresponding to 100 emitters within a single facilitation sphere) and a low pump rate $\kappa_p = \lambda/n_p(0)$, with $\lambda = 3.2 \times 10^{-3}$. The limit cycle persists for many cycles, exhibiting small variations in oscillation amplitude alongside a steady decrease in the pump-state density, until the dynamics halts when $n_p = n$.

IV. DISCUSSIONS AND CONCLUSION

To summarize, in this work, we demonstrate the emergence of quantum LCs that exhibit dynamical spatial correlations and entropy production in an open quantum system. The periodic long-range correlations originate from the multiplicative quantum noises inherent to the system and from the repeated sweeping through a tipping point. The features are captured qualitatively by a Gaussian-Floquet analysis and confirmed quantitatively by numerical simulations.

However, it is important to note that the long-range correlations stemming from the tipping point are insufficient to stabilize sustained oscillations—stable LCs are essential. Rather, it is the combined effects of three key elements: (1) the enhanced dynamical susceptibility near the tipping point; (2) the active seed generation through the rare spontaneous activation process; and (3) the independent local dissipation, which together produces the regular, periodic, back-and-forth collective switching between the absorbing and the active state. As our previous analysis indicates, the robustness of SOB-induced LCs is directly linked to the stability of first-order APTs under quantum fluctuations [50]. Therefore, in low spatial dimensions where first-order APTs are absent, the corresponding lack of tipping points precludes for the emergence of such dynamical synchrony among distant emitters.

By demonstrating how tipping points give rise to long-range correlations in strongly interacting driven-dissipative quantum many-body systems, our work extends the notion of critical thresholds and early-warning signals to the far-from-equilibrium quantum realm [51]. Moreover, it also shows how SOB—as a certain type of Hopf bifurcation [74,81]—can aid in stabilizing the phase coherence of LCs in diffusively coupled, spatially extended, and noisy systems through self-organized correlations.

ACKNOWLEDGMENTS

This work was supported by the National Natural Science Foundation of China (12347102 and 12547183), the Natural Science Foundation of Jiangsu Province (BK20233001), the Innovation Program for Quantum Science and Technology (2024ZD0300101), and the Fundamental and Interdisciplinary Disciplines Breakthrough Plan of the Ministry of Education of China (JYB2025XDXM502). The authors also acknowledge the computational resources provided by the High Performance Computing Center of Nanjing University.

DATA AVAILABILITY

There are no publicly available research data or software supporting this manuscript. Requests for further information or data should be sent to the authors.

[1] A. J. Lotka, Analytical note on certain rhythmic relations in organic systems, Proc. Natl. Acad. Sci. USA **6**, 410 (1920).

[2] V. Volterra, Fluctuations in the abundance of a species considered mathematically, Nature (London) **118**, 558 (1926).

[3] I. Prigogine and R. Lefever, Symmetry breaking instabilities in dissipative systems. II, J. Chem. Phys. **48**, 1695 (1968).

[4] R. Lefever and G. Nicolis, Chemical instabilities and sustained oscillations, J. Theor. Biol. **30**, 267 (1971).

[5] R. M. May, Biological populations with nonoverlapping generations: Stable points, stable cycles, and chaos, Science **186**, 645 (1974).

[6] R. M. Nisbet and W. S. Gurney, A simple mechanism for population cycles, Nature (London) **263**, 319 (1976).

[7] G. Ertl, Oscillatory kinetics and spatio-temporal self-organization in reactions at solid surfaces, Science **254**, 1750 (1991).

[8] I. R. Epstein and K. Showalter, Nonlinear chemical dynamics: Oscillations, patterns, and chaos, J. Phys. Chem. **100**, 13132 (1996).

[9] F. Baras, Stochastic analysis of limit cycle behavior in spatially extended systems, Phys. Rev. Lett. **77**, 1398 (1996).

[10] V. K. Vanag, L. Yang, M. Dolnik, A. M. Zhabotinsky, and I. R. Epstein, Oscillatory cluster patterns in a homogeneous chemical system with global feedback, Nature (London) **406**, 389 (2000).

[11] R. P. Boland, T. Galla, and A. J. McKane, How limit cycles and quasi-cycles are related in systems with intrinsic noise, J. Stat. Mech. (2008) P09001.

[12] R. P. Boland, T. Galla, and A. J. McKane, Limit cycles, complex Floquet multipliers, and intrinsic noise, Phys. Rev. E **79**, 051131 (2009).

[13] C.-K. Chan, T. E. Lee, and S. Gopalakrishnan, Limit-cycle phase in driven-dissipative spin systems, Phys. Rev. A **91**, 051601(R) (2015).

[14] K. Tucker, B. Zhu, R. J. Lewis-Swan, J. Marino, F. Jimenez, J. G. Restrepo, and A. M. Rey, Shattered time: Can a dissipative time crystal survive many-body correlations? New J. Phys. **20**, 123003 (2018).

[15] F. Piazza and H. Ritsch, Self-ordered limit cycles, chaos, and phase slippage with a superfluid inside an optical resonator, Phys. Rev. Lett. **115**, 163601 (2015).

[16] E. I. R. Chiacchio and A. Nunnenkamp, Dissipation-induced instabilities of a spinor Bose-Einstein condensate inside an optical cavity, Phys. Rev. Lett. **122**, 193605 (2019).

[17] D. Barberena, R. J. Lewis-Swan, J. K. Thompson, and A. M. Rey, Driven-dissipative quantum dynamics in ultra-long-lived dipoles in an optical cavity, Phys. Rev. A **99**, 053411 (2019).

[18] B. Zhu, J. Marino, N. Y. Yao, M. D. Lukin, and E. A. Demler, Dicke time crystals in driven-dissipative quantum many-body systems, New J. Phys. **21**, 073028 (2019).

[19] B. Buča, J. Tindall, and D. Jaksch, Non-stationary coherent quantum many-body dynamics through dissipation, Nat. Commun. **10**, 1730 (2019).

[20] B. Buča and D. Jaksch, Dissipation induced nonstationarity in a quantum gas, Phys. Rev. Lett. **123**, 260401 (2019).

[21] H. Keßler, J. G. Cosme, M. Hemmerling, L. Mathey, and A. Hemmerich, Emergent limit cycles and time crystal dynamics in an atom-cavity system, Phys. Rev. A **99**, 053605 (2019).

[22] N. Dogra, M. Landini, K. Kroeger, L. Hruby, T. Donner, and T. Esslinger, Dissipation-induced structural instability and chiral dynamics in a quantum gas, Science **366**, 1496 (2019).

[23] P. Kongkhambut, J. Skulte, L. Mathey, J. G. Cosme, A. Hemmerich, and H. Keßler, Observation of a continuous time crystal, Science **377**, 670 (2022).

[24] P. Gao, Z.-W. Zhou, G.-C. Guo, and X.-W. Luo, Self-organized limit cycles in red-detuned atom-cavity systems, Phys. Rev. A **107**, 023311 (2023).

[25] X. Wu, Z. Wang, F. Yang, R. Gao, C. Liang, M. K. Tey, X. Li, T. Pohl, and L. You, Dissipative time crystal in a strongly interacting Rydberg gas, Nat. Phys. **20**, 1389 (2024).

[26] D. Ding, Z. Bai, Z. Liu, B. Shi, G. Guo, W. Li, and C. S. Adams, Ergodicity breaking from Rydberg clusters in a driven-dissipative many-body system, Sci. Adv. **10**, eadl5893 (2024).

[27] Y. Jiao, Y. Zhang, J. Bai, S. Jia, C. S. Adams, Z. Bai, H. Shen, and J. Zhao, Photoionization-induced Floquet driving of a discrete time crystal in a thermal Rydberg ensemble, Phys. Rev. Lett. **135**, 163603 (2025).

[28] N. Träger, P. Gruszecki, F. Lisiecki, F. Groß, J. Förster, M. Weigand, H. Głowiński, P. Kuświk, J. Dubowik, G. Schütz, M. Krawczyk, and J. Gräfe, Real-space observation of magnon interaction with driven space-time crystals, Phys. Rev. Lett. **126**, 057201 (2021).

[29] P. Yang, M. Baggioli, Z. Cai, Y. Tian, and H. Zhang, Holographic dissipative spacetime supersolids, Phys. Rev. Lett. **131**, 221601 (2023).

[30] G. Žlabys, C.-h. Fan, E. Anisimovas, and K. Sacha, Six-dimensional time-space crystalline structures, Phys. Rev. B **103**, L100301 (2021).

[31] H. Bernien, S. Schwartz, A. Keesling, H. Levine, A. Omran, H. Pichler, S. Choi, A. S. Zibrov, M. Endres, M. Greiner, *et al.*, Probing many-body dynamics on a 51-atom quantum simulator, Nature (London) **551**, 579 (2017).

[32] J. Smits, L. Liao, H. T. C. Stoof, and P. van der Straten, Observation of a space-time crystal in a superfluid quantum gas, Phys. Rev. Lett. **121**, 185301 (2018).

[33] P. Geysermans and F. Baras, Stochastic description of a period-2 limit cycle, Europhys. Lett. **40**, 1 (1997).

[34] C. Navarrete-Benlloch, T. Weiss, S. Walter, and G. J. de Valcárcel, General linearized theory of quantum fluctuations around arbitrary limit cycles, Phys. Rev. Lett. **119**, 133601 (2017).

[35] A. Cabot, L. S. Muhle, F. Carollo, and I. Lesanovsky, Quantum trajectories of dissipative time crystals, Phys. Rev. A **108**, L041303 (2023).

[36] F. Carollo and I. Lesanovsky, Exact solution of a boundary time-crystal phase transition: Time-translation symmetry breaking and non-Markovian dynamics of correlations, Phys. Rev. A **105**, L040202 (2022).

[37] M. Marcuzzi, E. Levi, W. Li, J. P. Garrahan, B. Olmos, and I. Lesanovsky, Non-equilibrium universality in the dynamics of dissipative cold atomic gases, New J. Phys. **17**, 072003 (2015).

[38] M. Marcuzzi, M. Buchhold, S. Diehl, and I. Lesanovsky, Absorbing state phase transition with competing quantum and classical fluctuations, Phys. Rev. Lett. **116**, 245701 (2016).

[39] C. Pérez-Espigares, M. Marcuzzi, R. Gutiérrez, and I. Lesanovsky, Epidemic dynamics in open quantum spin systems, Phys. Rev. Lett. **119**, 140401 (2017).

[40] R. Gutiérrez, C. Simonelli, M. Archimi, F. Castellucci, E. Arimondo, D. Ciampini, M. Marcuzzi, I. Lesanovsky, and O. Morsch, Experimental signatures of an absorbing-state phase transition in an open driven many-body quantum system, Phys. Rev. A **96**, 041602(R) (2017).

[41] D. Roscher, S. Diehl, and M. Buchhold, Phenomenology of first-order dark-state phase transitions, Phys. Rev. A **98**, 062117 (2018).

[42] K. Klocke and M. Buchhold, Controlling excitation avalanches in driven Rydberg gases, Phys. Rev. A **99**, 053616 (2019).

[43] S. Helmrich, A. Arias, G. Lochead, T. M. Wintermantel, M. Buchhold, S. Diehl, and S. Whitlock, Signatures of self-organized criticality in an ultracold atomic gas, Nature (London) **577**, 481 (2020).

[44] E. Gillman, F. Carollo, and I. Lesanovsky, Quantum and classical temporal correlations in $(1+1)$D quantum cellular automata, Phys. Rev. Lett. **127**, 230502 (2021).

[45] T. Wintermantel, M. Buchhold, S. Shevate, M. Morgado, Y. Wang, G. Lochead, S. Diehl, and S. Whitlock, Epidemic growth and Griffiths effects on an emergent network of excited atoms, Nat. Commun. **12**, 103 (2021).

[46] D. Brady and M. Fleischhauer, Mean-field approach to Rydberg facilitation in a gas of atoms at high and low temperatures, Phys. Rev. A **108**, 052812 (2023).

[47] D. Brady, S. Ohler, J. Otterbach, and M. Fleischhauer, Anomalous directed percolation on a dynamic network using Rydberg facilitation, Phys. Rev. Lett. **133**, 173401 (2024).

[48] V. Buendía, S. di Santo, J. A. Bonachela, and M. A. Muñoz, Feedback mechanisms for self-organization to the edge of a phase transition, Front. Phys. **8**, 333 (2020).

[49] S. di Santo, R. Burioni, A. Vezzani, and M. A. Muñoz, Self-organized bistability associated with first-order phase transitions, Phys. Rev. Lett. **116**, 240601 (2016).

[50] Y.-X. Xiang, Q.-L. Lei, Z. Bai, and Y.-Q. Ma, Self-organized time crystal in driven-dissipative quantum system, Phys. Rev. Res. **6**, 033185 (2024).

[51] J. Zhang, L.-H. Zhang, B. Liu, Z.-Y. Zhang, S.-Y. Shao, Q. Li, H.-C. Chen, Z.-K. Liu, Y. Ma, T.-Y. Han, Q.-F. Wang, C. S. Adams, B.-S. Shi, and D.-S. Ding, Early warning signals of the tipping point in strongly interacting Rydberg atoms, Phys. Rev. Lett. **133**, 243601 (2024).

[52] A. J. Veraart, E. J. Faassen, V. Dakos, E. H. Van Nes, M. Lürling, and M. Scheffer, Recovery rates reflect distance to a tipping point in a living system, Nature (London) **481**, 357 (2012).

[53] E. H. van Nes and M. Scheffer, Slow recovery from perturbations as a generic indicator of a nearby catastrophic shift, Am. Nat. **169**, 738 (2007).

[54] M. Scheffer, J. Bascompte, W. A. Brock, V. Brovkin, S. R. Carpenter, V. Dakos, H. Held, E. H. van Nes, M. Rietkerk, and G. Sugihara, Early-warning signals for critical transitions, Nature (London) **461**, 53 (2009).

[55] L. Xu, D. Patterson, S. A. Levin, and J. Wang, Non-equilibrium early-warning signals for critical transitions in ecological systems, Proc. Natl. Acad. Sci. USA **120**, e2218663120 (2023).

[56] T. M. Lenton, H. Held, E. Kriegler, J. W. Hall, W. Lucht, S. Rahmstorf, and H. J. Schellnhuber, Tipping elements in the Earth's climate system, Proc. Natl. Acad. Sci. USA **105**, 1786 (2008).

[57] R. M. May, S. A. Levin, and G. Sugihara, Complex systems: Ecology for bankers, Nature (London) **451**, 893 (2008).

[58] J. Wang, L. Xu, and E. Wang, Potential landscape and flux framework of nonequilibrium networks: Robustness, dissipation, and coherence of biochemical oscillations, Proc. Natl. Acad. Sci. USA **105**, 12271 (2008).

[59] P. Zhou and T. Li, Construction of the landscape for multi-stable systems: Potential landscape, quasi-potential, A-type integral and beyond, J. Chem. Phys. **144**, 094109 (2016).

[60] H. Hinrichsen, Non-equilibrium phase transitions, Physica A **369**, 1 (2006).

[61] L. J. Wang, A. Kuzmich, and A. Dogariu, Gain-assisted superluminal light propagation, Nature (London) **406**, 277 (2000).

[62] L. Deng and M. G. Payne, Gain-assisted large and rapidly responding Kerr effect using a room-temperature active Raman gain medium, Phys. Rev. Lett. **98**, 253902 (2007).

[63] C. W. Gardiner, A. S. Parkins, and P. Zoller, Wave-function quantum stochastic differential equations and quantum-jump simulation methods, Phys. Rev. A **46**, 4363 (1992).

[64] C. Gardiner and P. Zoller, *Quantum Noise: A Handbook of Markovian and Non-Markovian Quantum Stochastic Methods with Applications to Quantum Optics* (Springer Science & Business Media, Berlin, Germany, 2004).

[65] M. Buchhold, B. Everest, M. Marcuzzi, I. Lesanovsky, and S. Diehl, Nonequilibrium effective field theory for absorbing state phase transitions in driven open quantum spin systems, Phys. Rev. B **95**, 014308 (2017).

[66] H.-K. Janssen, On a Lagrangean for classical field dynamics and renormalization group calculations of dynamical critical properties, Z. Phys. B **23**, 377 (1976).

[67] P. C. Martin, E. D. Siggia, and H. A. Rose, Statistical dynamics of classical systems, Phys. Rev. A **8**, 423 (1973).

[68] L. Onsager and S. Machlup, Fluctuations and irreversible processes, Phys. Rev. **91**, 1505 (1953).

[69] C. D. Dominicis, Techniques de renormalisation de la théorie des champs et dynamique des phénomenes critiques, J. Phys. Colloques **37**, C1-247 (1976).

[70] A. Kamenev, *Field Theory of Non-Equilibrium Systems*, 2nd ed. (Cambridge University Press, Cambridge, 2023).

[71] R. Zakine and E. Vanden-Eijnden, Minimum-action method for nonequilibrium phase transitions, Phys. Rev. X **13**, 041044 (2023).

[72] D.-S. Ding, H. Busche, B.-S. Shi, G.-C. Guo, and C. S. Adams, Phase diagram and self-organizing dynamics in a thermal ensemble of strongly interacting Rydberg atoms, Phys. Rev. X **10**, 021023 (2020).

[73] C. Wissel, A universal law of the characteristic return time near thresholds, Oecologia **65**, 101 (1984).

[74] S. H. Strogatz, *Dynamics and Chaos: Nonlinear With Applications to Physics, Biology, Chemistry, and Engineering*, 2nd ed (CRC Press, Boca Raton, FL, 2018).

[75] L. Pechenik and H. Levine, Interfacial velocity corrections due to multiplicative noise, Phys. Rev. E **59**, 3893 (1999).

[76] I. Dornic, H. Chaté, and M. A. Muñoz, Integration of Langevin equations with multiplicative noise and the viability of field theories for absorbing phase transitions, Phys. Rev. Lett. **94**, 100601 (2005).

[77] P. Ao, Potential in stochastic differential equations: Novel construction, J. Phys. A: Math. Gen. **37**, L25 (2004).

[78] P. Gaspard, Time-reversed dynamical entropy and irreversibility in Markovian random processes, J. Stat. Phys. **117**, 599 (2004).

[79] M. Doi, *Soft Matter Physics* (Oxford University Press, Oxford, 2013).

[80] L. Bertini, A. De Sole, D. Gabrielli, G. Jona-Lasinio, and C. Landim, Macroscopic fluctuation theory, Rev. Mod. Phys. **87**, 593 (2015).

[81] M. C. Cross and P. C. Hohenberg, Pattern formation outside of equilibrium, Rev. Mod. Phys. **65**, 851 (1993).